PERGAMON

Aerosol Science 33 (2002) 1–16

Journal of
Aerosol Science

www.elsevier.com/locate/jaerosci

Coalescence enhanced synthesis of nanoparticles to control size, morphology and crystalline phase at high concentrations

Donggeun Lee, Mansoo Choi *

School of Mechanical and Aerospace Engineering, National CRI Center for Nano Particle Control, Seoul National University, Seoul, 151-742, South Korea

Received 16 February 2001; accepted 29 May 2001

Abstract

Size, morphology, and crystalline phase of nanoparticles determine the properties of nanostructured materials. Therefore, the mastery of controlling properties ultimately requires the control of size, morphology, and phase of nanoparticles. From various aerosol methods, highly pure nanoparticles can be produced; however, agglomeration has been considered as almost unavoidable when nanoparticles are generated at high concentrations that are necessary for a practical application. Efforts to control agglomeration have had only limited success. Here we report that the enhancement of coalescence of nanoparticles using laser beam irradiation on aggregates formed in flames can be a solution for this problem and successfully controls the size, morphology, and crystalline phase of high concentration nanoparticles of silica and titania. We demonstrate this principle by not only synthesizing smaller and unagglomerated nanoparticles, but also generating them in high concentrations. In addition, we show that the present method is capable of even controlling the crystalline phase of titania nanoparticles. Surprisingly, stable rutile titania particles have been transformed into metastable anatase and the weight percent of each phase could be controlled.

Keywords: Nanoparticles; Laser irradiation; Coalescence; Size control

1. Introduction

Nanophase materials including crystalline and non-crystalline nanoparticles have great potentials for applications in various industrial areas such as nanoceramics, catalysts, electronics, metallurgy, optical and magnetic devices. Nanocrystalline particles may have different applications depending on their crystalline phases. For example, anatase titania particles have been proved to be more active photocatalysts in environmental remediation than rutile

* Corresponding author. Tel.: +82-2-880-7128; fax: +82-2-883-0179.
E-mail address: mchoi@plaza.snu.ac.kr (M. Choi).

0021-8502/01/$ - see front matter
PII: S0021-8502(01)00155-0

(Fox & Dulay, 1993) while rutile particles have been used as a white pigment (Mezey, 1966). Moreover, nanostructured materials made from nanoparticles have attracted much interest in recent years due to their unusual properties and excellent sinterability compared to conventional coarse-grained materials (Gleiter, 1989; Siegel, 1994). Size, morphology, and crystalline phase of nanoparticles determine the properties of nanostructured materials. Therefore, the mastery of controlling properties ultimately requires the control of size, morphology, and phase of nanoparticles. In many cases, smaller and unagglomerated particles are desirable for compacting and subsequent sintering processes to synthesize high quality nanostructure materials. Gas phase methods generally produce purer nanoparticles than liquid based processes since even the purest water contains traces of minerals (Kruis, Fissan, & Peled, 1998). Meanwhile, the most prominent problem of gas phase methods is poor controllability in growth of nanoparticles especially when nanoparticles are generated at high concentrations which are needed for practical applications.

The morphology and size of particles are determined by the competition between collision and coalescence of particles (Windeler, Friedlander, & Lehtinen, 1997). The function of aggregates is due to faster collision of particles than coalescence. Even though the method of salt addition to coat on particles generated in a flame had been shown to produce unagglomerated nanoparticles (DuFaux & Axelbaum, 1995), high purity of particles could not be obtained and the subsequent process of washing may pose an additional problem of agglomeration. The electrical field had been applied in a particle generating flame to successfully control the size of primary particles and aggregates; however, the formation of aggregates could not be avoided (Vemury & Pratsinis, 1995). More detailed experiment on electrical field effects was done recently (Katzer, Weber, & Kasper, 2000).

Recently, we attempted to irradiate CO_2 laser beam on aggregates forming in a flame for the purpose of controlling size and morphology of amorphous silica nanoparticles. It was found from local thermophoretic sampling and TEM image analysis that the laser irradiation in a flame could produce much smaller and at the same time spherical silica nanoparticles and affect the growth of silica particles differently depending on the irradiation height (Lee & Choi, 2000). In the present study, the method using laser irradiation on aggregates that form in a flame is extended to the synthesis of crystalline nanoparticles to examine the controllability of the crystalline phase of nanoparticles as well as the size and morphology. The validity of this method, named here as coalescence enhanced synthesis, is quantitatively verified by measuring the changes of number density, volume fraction, and size distributions with and without laser irradiation. Our method relies on controlling the characteristic time for coalescence of nanoparticles (Seto, Hirota, Fujimoto, Shimada, & Okuyama, 1997; Ehrman, Friedlander, & Zachariah, 1998; Lee, Jeong, Hwang, Choi, & Chung, 2001; Jeong & Choi, 2001) by irradiating CO_2 laser beam on the early stage aggregates formed during flame synthesis. As shown in Fig. 1, small aggregates that begin to form in a flame are irradiated by a high power CW CO_2 laser beam to rapidly coalesce and change into spheres. Since spherical particles have much smaller collision cross sections than volume equivalent aggregates (Windeler et al., 1997; Matsoukas & Friedlander, 1991), much slower growth of nanoparticles can be achieved. We estimated the change of collision frequency β's before and after transforming aggregates into volume equivalent spheres using Eq. (3) suggested in the paper of Matsoukas and Friedlander (1991). The collision frequency function of the transformed spheres is estimated to be reduced to about 30% of the original value

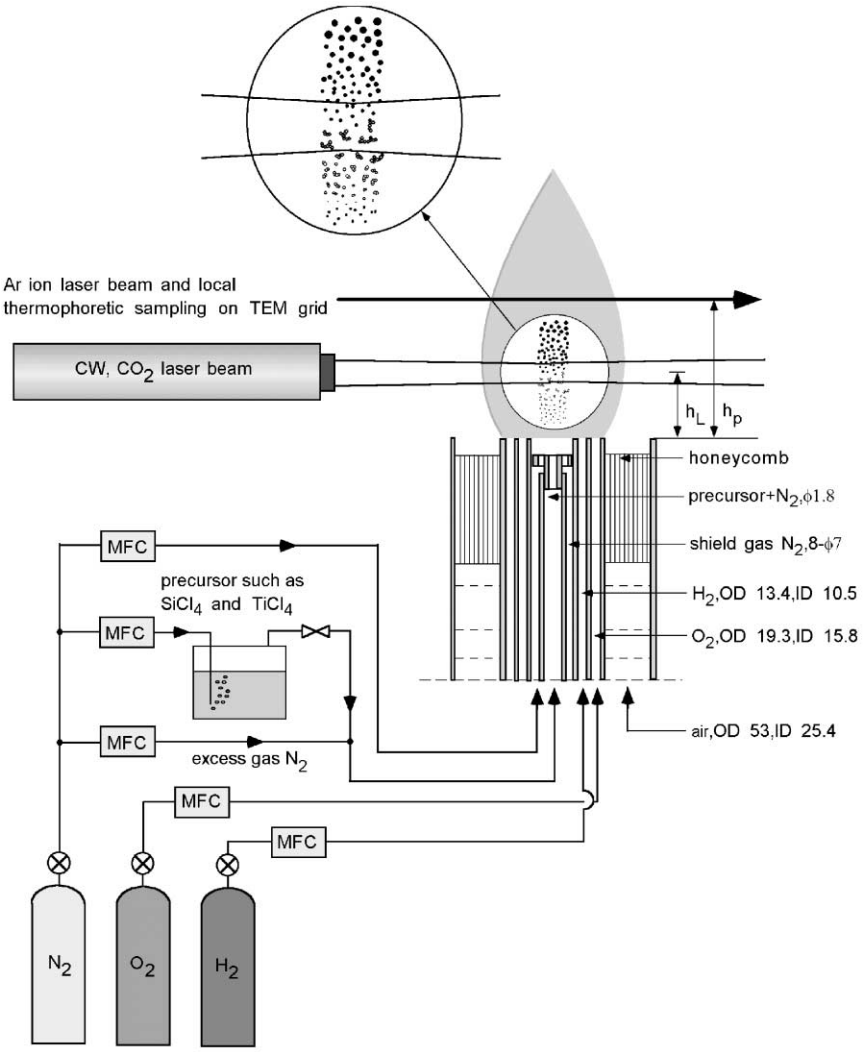

Fig. 1. Schematic of coalescence enhanced synthesis for smaller and unagglomerated nanoparticles with controlled crystallinity at high concentrations: OD (outer diameter of annular space (mm)); ID (inner diameter (mm)).

for a sample aggregate, $D_f = 1.5$ and $N_p = 5$. Considering that the particle growth is a result of multiple collisions, this reduction should affect the particle growth significantly. Therefore, much smaller and unagglomerated spherical particles could be obtained with the simultaneous increase of number density. Rapid heating of nanoparticles due to the irradiation of laser beam and subsequent cooling after passing the irradiation zone have been utilized to control the crystalline phase of nanocrystalline particles. Variations of number density and volume fraction as well as the variation of sizes and shapes of both silica and titania nanoparticles with different laser powers are quantitatively measured using Mie scattering theory, Rayleigh–Debye–Gans/Fractal

Aggregate (RDG/FA) scattering theory and TEM image analysis for locally captured particles (Cho & Choi, 2000). The change of crystalline phase of TiO_2 nanoparticles has also been investigated using X-ray diffraction (XRD).

2. Experimental

2.1. Experimental apparatus and instrumentation

Fig. 1 shows an experimental setup which consists of a burner, two laser beams for particle heating and light scattering measurement, respectively, and a local thermophoretic sampling. A laminar diffusion flame burner composed of six concentric stainless-steel tubes (Hwang, Gil, Kim, Choi, & Chung, 2001) was used. SiO_2 and TiO_2 particles are generated in an oxy-hydrogen diffusion flame by hydrolysis and oxidation of $SiCl_4$ and $TiCl_4$, respectively. Laser light scattering experiments are conducted using Ar ion laser beam (514.5 nm in wavelength) and a high power CW CO_2 laser (10.6 μm) is employed to rapidly heat aggregates forming in a flame. The experimental apparatus has been described in detail in our previous paper (refer to Lee & Choi, 2000). Note that the CO_2 laser irradiation height from the burner surface (h_L) is positioned below the height (h_p) where Ar ion light scattering measurement and local sampling are done. Liquid $TiCl_4$ in a bubbler (Aldrich, 99.9%) is maintained at 40°C or above while $SiCl_4$ is maintained at 26°C.

TiO_2 particles moving along the flame are thermophoretically collected by a water-cooled quartz tube (6 mm in outer diameter and 300 mm in length) for further examination of crystallinity. The heights from the burner surface where the quartz tube is located have been adjusted precisely with 2D traversing system. TiO_2 particles are deposited for only 1–2 min to prevent undesirable excessive heating of the deposited layer and then removed for subsequent X-ray diffraction measurement. This procedure is repeated before collecting approximately 80 mg of powders.

2.2. Determination of number density and volume fraction of spherical and aggregate particles

The mean volumetric differential scattering coefficient Q_{vv} is estimated from the measured scattered intensity after calibrating the system response using a propane gas (Choi, Cho, Lee, & Kim, 1999).

For spherical particles, Q_{vv} can be expressed as follows by integrating over all sizes:

$$Q_{vv}(\vartheta) = N_s \int C_{vv}(X_p, \vartheta) f(d_p)\, \mathrm{d}d_p, \tag{1}$$

where $C_{vv}(X_p, \theta)$ is the differential scattering cross section of a spherical particle calculated from the Mie theory, N_s is the number density of spheres, and X_p is the optical size parameter (defined as $\pi d_p/\lambda$). In the present study, the probability density function of spherical particle

sizes, $f(d_p)$ is assumed approximately as log-normal.

$$f(d_p) = \frac{1}{\sqrt{2\pi} d_p \ln(\sigma_g)} \exp\left[-\frac{(\ln(d_p) - \ln(d_g))^2}{2(\ln(\sigma_g))^2}\right], \tag{2}$$

where d_g and σ_g are the geometric mean diameter and the geometric standard deviation, respectively, that can be determined from local thermophoretic sampling and TEM image analysis. Once $f(d_p)$ is determined, the total number density of spherical particle, N_s can be easily determined from Eq. (1). The volume fraction f_v, is simply calculated from the following equation:

$$f_v = N_s \frac{\pi}{6} \int d_p^3 f(d_p)\, \mathrm{d}d_p = N_s \frac{\pi}{6} D_{30}^3 \tag{3}$$

where D_{30} is the volume mean diameter of particles.

For fractal-like aggregates, the Rayleigh–Debye–Gans/Fractal-Aggregate (RDG/FA) theory (Sorensen, Cai, & Lu, 1992; Koylu & Faeth, 1994; Farias, Carvalho, Koylu, & Faeth, 1995; Farias, Koylu, & Carvalho, 1996) combined with the local thermophoretic sampling and TEM image analysis (Cho & Choi, 2000) was applied to obtain the number density and volume fraction of TiO_2 aggregates.

The complex morphology of aggregates with a wide range of size and shape can be characterized by utilizing the concept of mass fractals which satisfy the following relationship between the number of primary particles per aggregate N_p, and its radius of gyration R_g (Jullien & Botet, 1987):

$$N_p = k_g \left(\frac{2R_g}{d_{pm}}\right)^{D_f}, \tag{4}$$

where k_g, d_{pm}, R_g and D_f are the fractal prefactor, the mean primary particle diameter, the radius of gyration and the fractal dimension, respectively. N_p can be determined from measuring the projected-area-equivalent diameter d_a through TEM image analysis (Koylu, Faeth, Farias, & Carvalho, 1995a). R_g, K_g, and D_f are also determined from the TEM image analysis (Koylu et al., 1995a; Koylu, Xing, & Rosner, 1995b). The mean volumetric differential scattering coefficient of randomly oriented polydisperse aggregates, Q_{vv}, can be expressed by integrating over all aggregate sizes.

$$Q_{vv}(\vartheta) = N_a \int C_{vv}^a(\vartheta) f(N_p)\, \mathrm{d}N_p, \tag{5}$$

where N_a is the number density of aggregates, and C_{vv}^a is the differential scattering cross section of a fractal-like aggregate. From the RDG/FA theory, C_{vv}^a can be expressed as follows (Jullien & Botet, 1987; Martin & Hurd, 1987; Dobbins & Megaridis, 1991):

$$C_{vv}^a(\vartheta) = N_p^2 C_{vv}^p(X_p\, \vartheta) \exp\left(-\frac{(qR_g)^2}{3}\right) \quad \text{for } qR_g < 1.5D_f \text{ (Guinier regime)} \tag{6a}$$

$$= N_p^2 C_{vv}^p(X_p, \theta)(qR_g)^{-D_f} \quad \text{for } qR_g > 1.5D_f \text{ (power-law regime)}, \tag{6b}$$

where C_{vv}^{p} is the differential scattering cross section of a primary particle (assuming that primary particles are spheres of the same size) and q is the modulus of scattering vector ($=4\pi/\lambda \sin(\theta/2)$). The probability density function of aggregate sizes, $f(N_p)$, can be assumed as log-normal:

$$f(N_p) = \frac{1}{\sqrt{2\pi} N_p \ln(\sigma_g)} \exp\left[-\frac{(\ln(N_p) - \ln(N_g))^2}{2(\ln(\sigma_g))^2}\right], \tag{7}$$

where N_g is the geometric mean number of primary particle per aggregate and σ_g is the geometric standard deviation of aggregate size that can be determined for TEM image analysis. Once $f(N_p)$ is determined, the number density of aggregates N_a, can be obtained from Eq. (5). The volume fraction f_v, is easily calculated from the following expression:

$$f_v = N_a \frac{\pi}{6} d_{pm}^3 \int N_p f(N_p)\, dN_p = N_a \frac{\pi}{6} D_{30}^3. \tag{8}$$

2.3. Determination of crystallinity of TiO_2 particles

The crystalline phase of the collected TiO_2 particles was determined by X-ray diffraction (MAC/Science, MXP18XHF-22) using Cu K_α radiation ($\lambda = 1.54056$ Å). Both nanocrystalline samples and reference materials were measured at a step width of 0.01° for a typical count time of 12 s. The K_{α_2} component of the scattering of Cu K_α radiation (1.5444 Å) was removed using the Rachinger algorithm (Klug & Alexander, 1974). Two different coarse-grained samples were used as standard samples to correct the instrumental broadening function of the diffractometer: first, well annealed rutile power (99%, Aldrich, particle size of $\sim$ 400 nm, originally anatase powder which fully transforms to rutile by heating for 12 h at 1300°C in air); second, bulk standard Si (Polycrystalline, supplied by MAC/Science). The weight fractions of the rutile phases in the samples are calculated from the relative intensities of the strongest peaks representing anatase ($2\theta = 25.3^\circ$ for the (1 0 1) reflection) and rutile ($2\theta = 27.5^\circ$ for the (1 1 0) reflection) peaks (Spurr & Myers, 1957).

3. Results and discussion

3.1. Control of size and morphology of SiO_2 particles

Fig. 2 shows the evolution of SiO_2 nanoparticles along the flame height under the condition in Table 1 without CO_2 laser beam irradiation (a1–a4 and b1) and the changes of spherical particle sizes depending on laser powers (b1, b2, b3 and b4). Aggregates composed of small primary particles begin to form at a distance of 14 mm from the burner surface (Fig. 2(a3)). The fast coalescence process of SiO_2 aggregate particles is clearly observed in Fig. 2(a4) and Fig. 2(b1) and aggregates are finally sintered to become more-spherical particles at 19 mm (note that some of the particles in Fig. 2(b1) still have a non-spherical shape). When CO_2 laser beam (3.3 mm in beam diameter) irradiates at 14 mm where aggregates begin to form, the sizes of

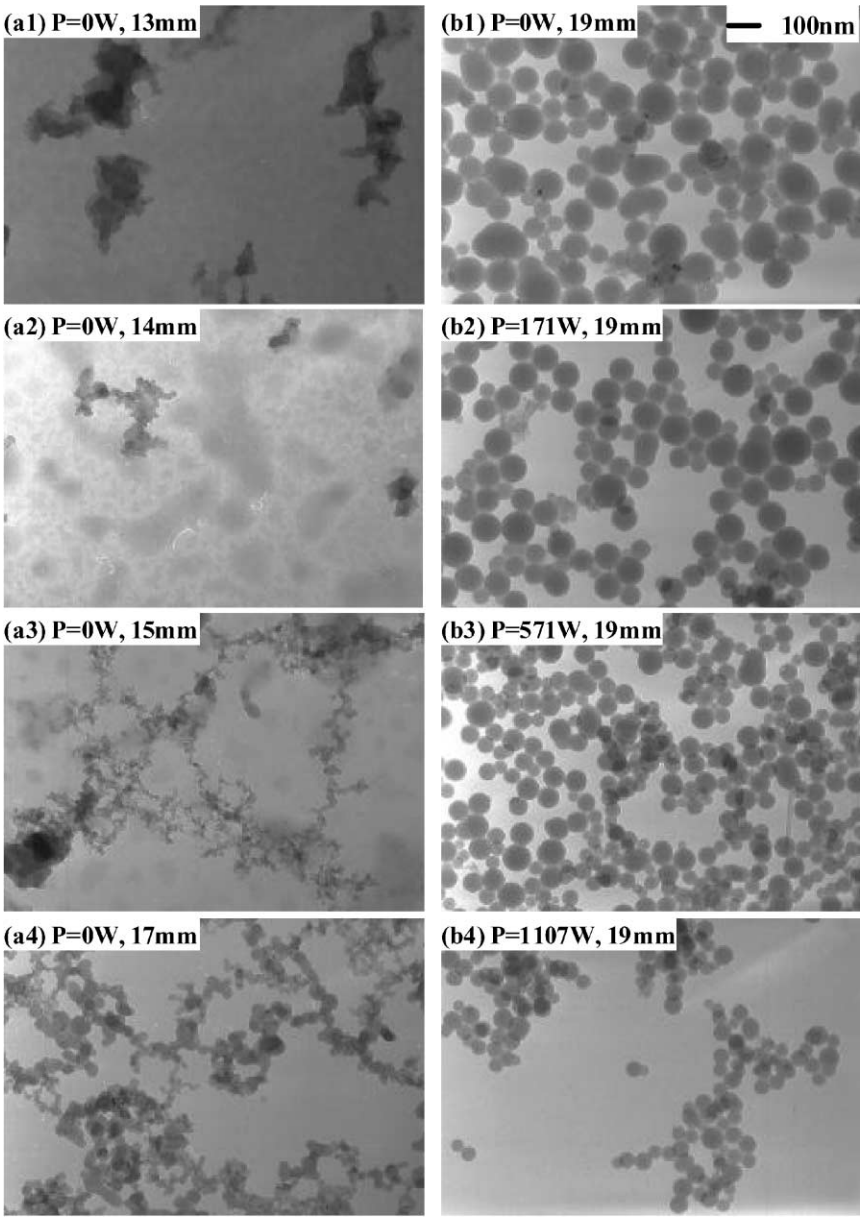

Fig. 2. TEM photographs for the evolution of SiO_2 particles with and without CO_2 laser beams; $h_L = 14$ mm, $h_p = 19$ mm.

particles captured at the flame height of 19 mm decrease monotonically maintaining spherical shape with laser power (Figs. 2(b1)–(b4)). The materials shown in Fig. 2(a1) would not be silica particles, but intermediate materials such as SiO and SiOH, which was also noted in Lee and Choi (2000).

Table 1
Experimental conditions

Experimental conditions	For SiO_2	For TiO_2
Carrier gas N_2 (cc/min)	75	100
Dilution gas N_2 (cc/min)	113	222.8
$SiCl_4$ or $TiCl_4$ vapor (cc/min)	37	3.5
Q_{total} (cc/min)	225	326.3
Shield gas N_2 (cc/min)	400	700
H_2 (l/min)	2.5	2.5
O_2 (l/min)	5.0	5.0
Dry air (l/min)	70	70
$SiCl_4$ or $TiCl_4$ vapor (mol/min)	1.5×10^{-3}	1.4×10^{-4}
Precursor jet exit velocity (m/s)[a]	1.47	2.14

[a]The velocity through the center nozzle of this burner (1.8 mm in diameter) is calculated at room temperature.

Fig. 3(a) shows the variations of particles geometric mean size determined from TEM image analysis of locally captured particles, which again confirms the considerable reduction of particle mean diameter from about 90 nm to less than 50 nm. At the same time, the volumetric scattering coefficient Q_{vv} of particles at 19 mm decreases substantially with CO_2 laser powers; Q_{vv} decreases up to about 1% of the original value of the case without CO_2 laser irradiation. From TEM image analysis, the size distributions of particles shown in Figs. 2(b1)–(b4) are found to be well approximated by log-normal size distributions (see Fig. 3(b)). The corresponding geometric standard deviations are found to decrease monotonically from 1.4 ($P = 0$ W) to 1.2 ($P = 1107$ W). Fig. 3(b) shows clearly that the probability density function for volume distribution of spherical particles becomes narrower with increasing laser powers. The possible explanation on how this can occur will be discussed later.

The volume fraction and number density of silica particles have been estimated as shown in Fig. 4 by using the Mie scattering theory and the measured log-normal distributions. For CO_2 laser powers below 257 W, the number density rapidly increases up to about three times the original value obtained without the irradiation while volume fraction of particles does not change much (number densities $= 4.2 \times 10^9$/cc for $P = 0$ W and 1.3×10^{10}/cc for $P = 257$ W). The substantial reduction of collision cross sections for volume equivalent spherical particles transformed from early stage aggregates near 14 mm would be the reason why the number density increases and at the same time, the sizes of particles captured at 19 mm decreases. Volume fraction should not change much since coalescence and collision of particles cannot alter the total volume fraction of particles. These data strongly support the validity of the present principle. For higher powers of CO_2 laser, both number density and volume fraction decrease due to the evaporation or thermal dissociation of silica particles that can occur even below the boiling point of silica particles (Emel'yanov, Konov, Tokarev, & Seminogov, 1989; Bailar, Emeleus, Nyholm, & Dickenson, 1973). However, number densities are still higher than the original case without CO_2 irradiation (see Fig. 4), which indicates that both coalescence and evaporation effects contribute to the size reduction of silica particles for high laser powers. Evaporation or thermal dissociation may be the possible cause why the size distributions (see

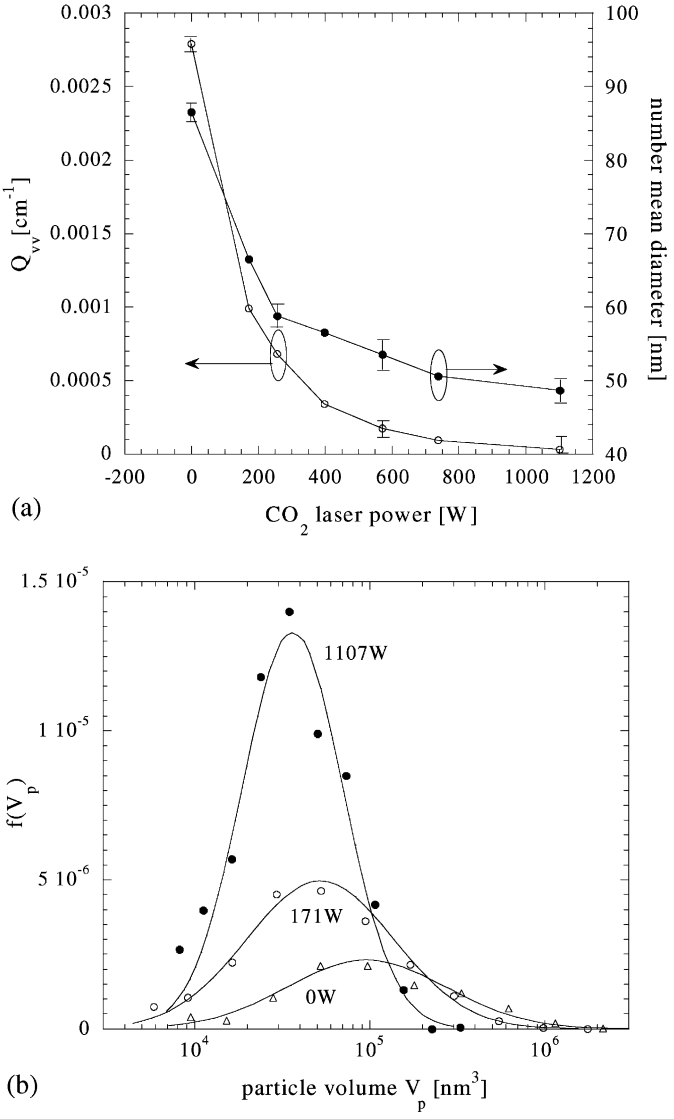

Fig. 3. (a) Variations of volumetric scattering coefficient and mean diameters of SiO_2 particles: 1000 or more particles were averaged in each case (b) variations of volume distribution of particles with CO_2 laser powers.

Fig. 3(b)) becomes narrower for high laser powers since the temperature increment due to the irradiation may be larger for larger particles so that larger particles may be thermally dissociated more easily than smaller particles (Lee & Choi, 2000).

Experimental errors for estimating number density and volume fraction are mostly resulting from the accuracy of the fitted size distribution of particles. Since the scattered light intensity is strongly affected by larger particles rather than smaller ones, a slight difference of the large-side tail in the log-normal size distribution may lead to a considerable uncertainty. In the present study, the maximum uncertainty is estimated to be 19% (95% confidence).

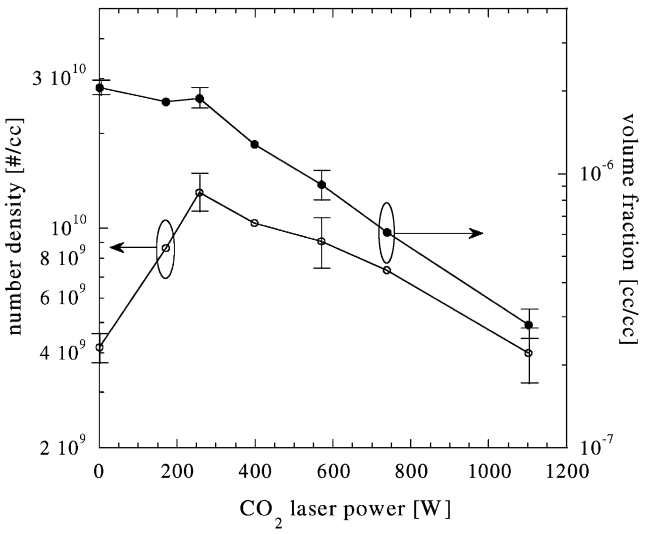

Fig. 4. Variations of number density and volume fraction of SiO_2 particles for different laser powers; $h_L = 14$ mm, $h_p = 19$ mm.

3.2. Control of size, morphology and crystalline phase of TiO_2 particles

Coalescence enhanced method using laser irradiation on aggregates forming in a flame is also applied to examine the possibility of controlling crystalline phase as well as controlling the size and morphology. Fig. 5 shows the change of size and morphology of titania particles captured at 18 mm with or without laser beam irradiated at 15 mm. Aggregates composed of 11 nm diameter primary particles appear at a distance of 18 mm from the burner surface without CO_2 laser irradiation (Fig. 5(a)). Under the CO_2 laser irradiation ($P = 2408$ W) at 15 mm, coalescence is obviously enhanced and thus original aggregates are transformed into much smaller 20 nm unagglomerated spherical particles (compare Fig. 5(a) and (b)). The magnified TEM image indicates that seemingly agglomerate particles in Fig. 5(b) turn out to be just a multiple deposition of isolated sphere particles on TEM grid. With laser irradiation, projected area equivalent diameters significantly decrease (projected area equivalent diameters: 110 nm for $P = 0$ W and 20 nm for $P = 2408$ W).

Fig. 6(a) shows the size distribution of aggregates which originally exist at the height h_p of 18 mm as a function of N_p. The size distribution of aggregates is well fitted into a log-normal profile (solid line in Fig. 6(a)), which supports the validity of the assumption of Eq. (7). Fig. 6(b) shows the number of primary particles (N_p) in an aggregate as a function of its normalized outer diameter (L^a/d_{pm}) for aggregates captured at 18 mm without CO_2 laser irradiation; size parameters of fractal aggregates can be determined from this plot as $D_f = 1.60$ and $k_g = 2.56$ (refer to Koylu et al., 1995a; 1995b). Note also in Fig. 7 that unagglomerated spherical titania particles collected at 18 mm with CO_2 irradiation at 15 mm also fit into a log-normal distribution. The number density (N_a) and volume fraction (f_v) of the original aggregates (see Fig. 5(a)) are estimated from the Rayleigh–Debye–Gans/Fractal Aggregate scattering theory to

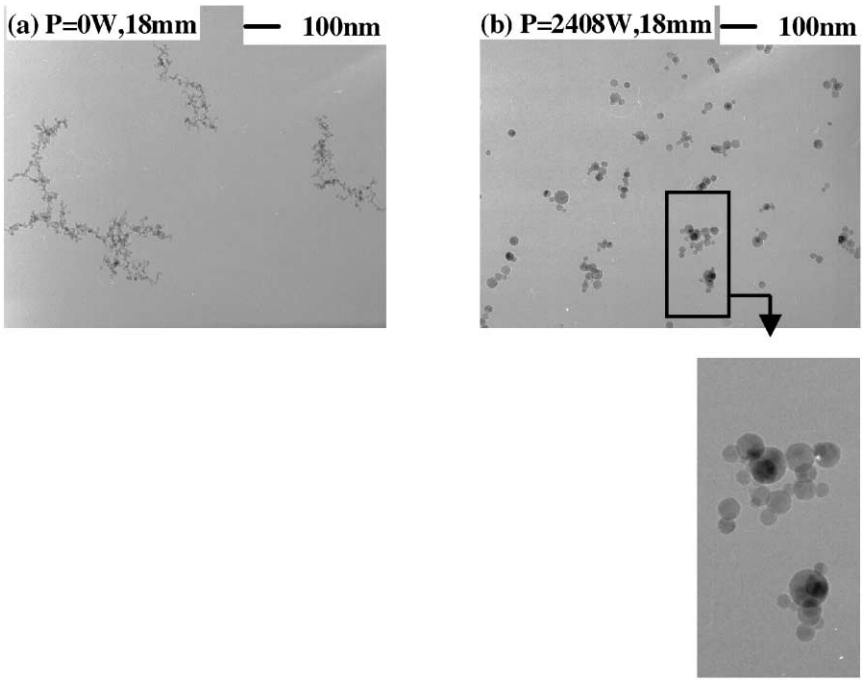

Fig. 5. TEM photographs showing the change of morphology and size of TiO_2 particles with or without CO_2 laser irradiation; $h_L = 15$ mm, $h_p = 18$ mm.

be 1.8×10^9 [/cc] and 2.7×10^{-7} [cc/cc], respectively, while N_s and f_v for the spheres (Fig. 5(b)) are 3.8×10^{10} and 2.5×10^{-7}, respectively. The number density of particles rapidly increases by 21 times the original value obtained without the irradiation while the volume fraction of particles does not vary significantly. This implies that TiO_2 particles within the laser beam would not be easily dissociated even at this high laser power while SiO_2 is known to be thermally dissociated even below its evaporation temperature (Bailar et al., 1973). The substantial reduction of collision cross sections of particles due to the enhancement of coalescence not only decreases particle sizes, but also increases the number density at 18 mm due to lower collision probability. Volume fraction should not decrease significantly since coalescence and collision of particles cannot alter the total volume fraction of particles. Furthermore, it is found that the average volume of particles has been greatly decreased by about 24 times; the volume mean diameter of original aggregates (Fig. 5(a)) and spheres (Fig. 5(b)) are 65.6 and 22.6 nm, respectively. This confirms that the present method is not just transforming aggregates into spheres, but synthesizing much smaller, at the same time, unagglomerated spherical titania by the reduction of collision cross sections of particles. CO_2 laser beam irradiation near 15 mm enhances rapidly the coalescence of early stage aggregates formed near 15 mm and transforms them into spherical particles that have much smaller collision cross sections than the original aggregates. Therefore, particle growth is retarded to finally produce much smaller sizes maintaining spherical shapes at 18 mm.

The controllability of crystalline phase has also been investigated. Fig. 8 shows XRD profiles of TiO_2 particles collected at 65 mm for different laser powers when the laser beam is irradiated

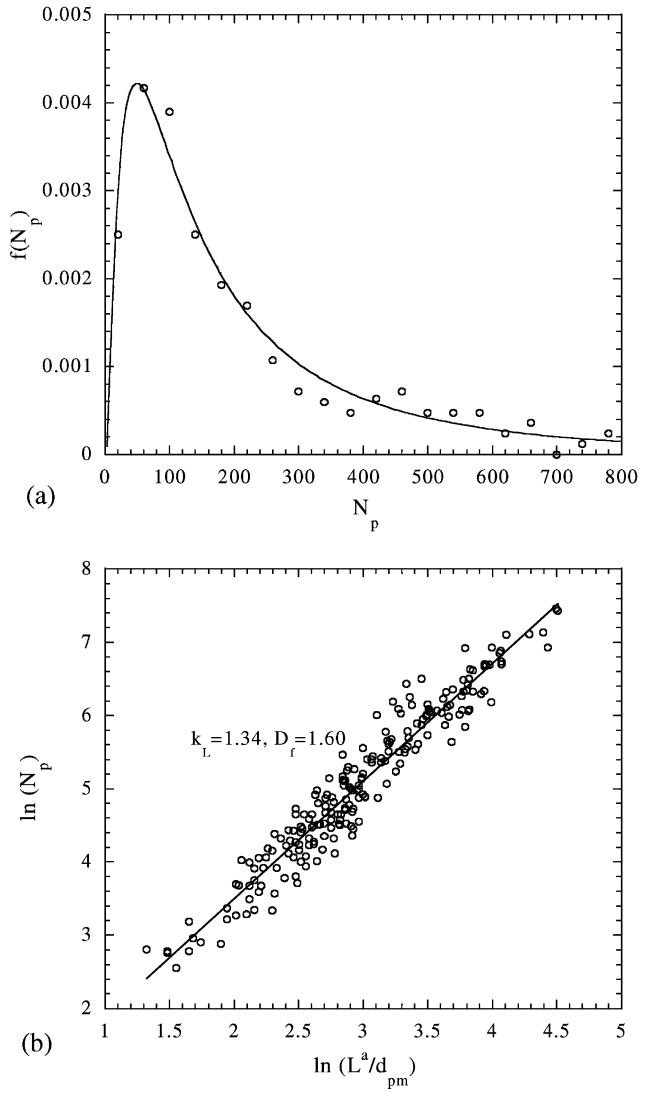

Fig. 6. (a) Probability density function of aggregates and (b) fractal characteristics of TiO_2 aggregate particles without CO_2 laser irradiation; $h_p = 18$ mm.

at 25 mm. In the figure, A and R denote Brag peaks of anatase and rutile, respectively. It is very interesting that rutile contents decrease monotonically with the increase of laser power. Even for different CO_2 laser irradiation positions, the trend of decreasing rutile weight percent is the same, although the decrements of the rutile contents are different depending on the irradiation heights (see Fig. 9). For sufficiently high laser powers, rutile peaks completely disappear. From this result, one may imagine that the laser irradiation results in the transformation of rutile into anatase, which is known to be impossible (Shannon & Pask, 1965). Zhang and Banfield (1998) proved from the thermodynamic analysis that rutile is the only thermodynamically stable

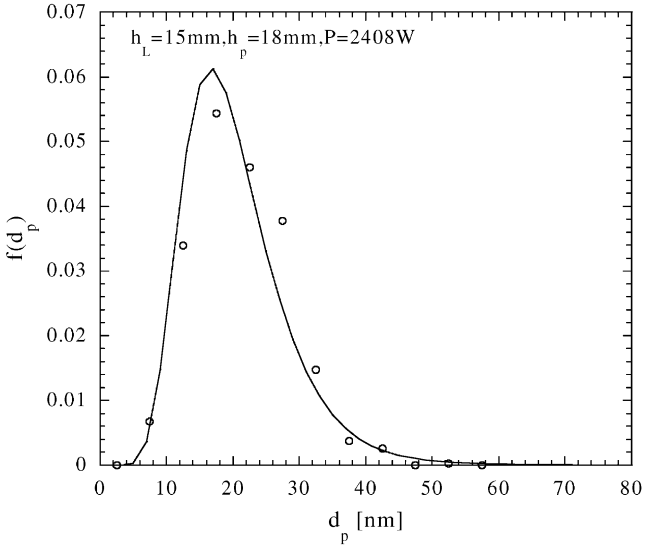

Fig. 7. Probability density function of TiO_2 spherical particles with CO_2 laser irradiation; $h_p = 18$ mm ($h_L = 15$ mm, $P = 2408$ W).

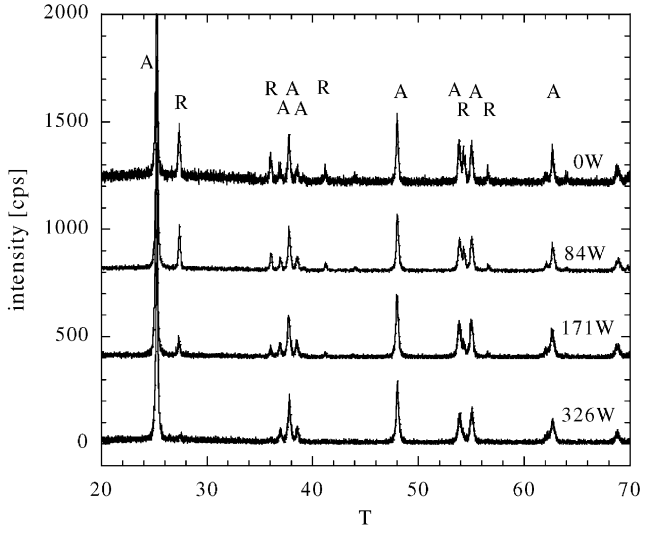

Fig. 8. Variations of XRD profiles of TiO_2 particles for different CO_2 laser powers; $h_L = 25$ mm, $h_p = 65$ mm.

phase when particle size exceeds 14 nm. Moreover, almost all previous researchers (Gribb & Banfield, 1997; Ding & Liu, 1996; Shannon & Pask, 1964) reported that the transformation from anatase to rutile was enhanced as the calcination temperature increased. In the absence of CO_2 laser irradiation, rutile weight percent increases monotonically with flame height; 2.6% at 15 mm, 6.9% at 20 mm, 10.3% at 25 mm, 13.3% at 40 mm and 16.6% at 65 mm. This is

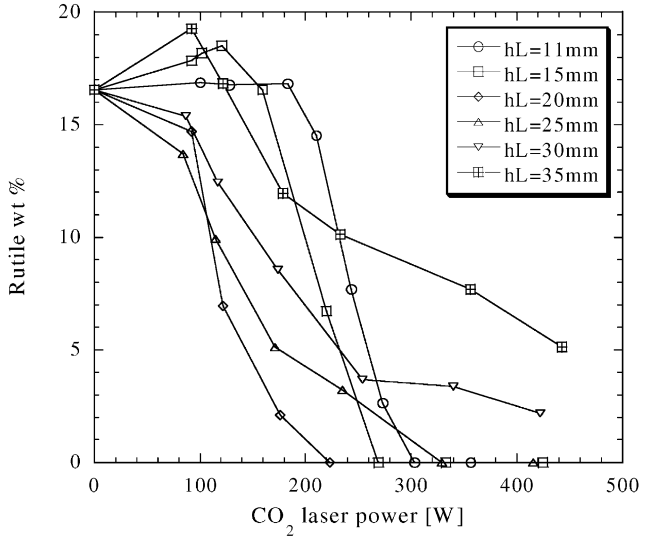

Fig. 9. Variations of rutile content in TiO_2 particles for different CO_2 laser powers and different irradiation positions; $h_p = 65$ mm.

consistent with previous studies. However, the present study using CO_2 laser irradiation reveals that the laser irradiation can alter the phase from rutile to anatase. For example, 16.6% rutile wt% in particles collected at 65 mm without CO_2 laser irradiation is now changed to almost 0% when CO_2 laser beam is irradiated at 25 mm with $P = 326$ W (see Figs. 8 and 9). It is emphasized that the original rutile content at 25 mm without laser irradiation is 10.3%. This indicates that the rutile particles at 25 mm could be transformed into anatase due to the laser irradiation. This result can be explained by the possible occurrence of melting due to irradiation and subsequent recrystallization after passing the irradiation zone (beam diameter: 3.3 mm). Sufficiently long time is necessary for atomic rearrangement leading to a more compact and stable rutile phase, but the cooling time in our system is very short, in the order of 1 ms. Therefore, the initial solid phase that can be recrystallized from melted titania might prefer metastable anatase phase (Gribb & Banfield, 1997). Furthermore, melting process should reduce necking area of aggregates, correspondingly, decrease the surface free energy which has been considered as a driving force to transform anatase to rutile (Gribb & Banfield, 1997; Zhang & Banfield, 1999). Therefore, more stabilized anatase phase could be produced and this may be one of the reasons why anatase particles recrystallized at the low irradiation position of 11 mm maintain their phase even after reaching the collecting position (65 mm).

4. Conclusions

Coalescence enhanced synthesis of nanoparticles using laser beam irradiation on aggregates formed in flames was shown to successfully control the size, morphology, and crystalline phase of high concentration nanoparticles. We demonstrated the validity of this principle by not only

synthesizing smaller and unagglomerated silica and titania nanoparticles, but also generating them in high concentrations. Therefore, this method manipulating the characteristic time for coalescence of nanoparticles could be one solution for the aggregation problem that occurs when nanoparticles are generated at high concentrations. In addition, we show that the present method is capable of even controlling the crystalline phase of titania nanoparticles. Surprisingly, stable rutile titania particles have been transformed into metastable anatase and the wt% of each phase could be controlled. This principle seems to be applicable to the synthesis of other single or multicomponent unagglomerated nanoparticles at high concentrations and may be extended to other gas phase methods as well as flame synthesis.

Acknowledgements

This work was funded by the Creative Research Initiatives Program supported by the Ministry of Science and Technology, Korea and also supported by the Brain Korea 21 Project.

References

Bailar, J. C., Emeleus, H. J., Nyholm, S. R., & Dickenson, A. F. T. (1973). *Comprehensive inorganic chemistry* (1st ed.), Vol. 1. Oxford: Pergamon press.

Cho, J., & Choi, M. (2000). Determination of number density, size and morphology of aggregates in coflow diffusion flame using light scattering and local sampling. *Journal of Aerosol Science*, *31* (9), 1077–1095.

Choi, M., Cho, J., Lee, J., & Kim, H. W. (1999). Measurements of silica aggregate particle growth using light scattering and thermophoretic sampling in a coflow diffusion flame. *Journal of Nanoparticle Research*, *1*, 169–183.

Ding, X.-Z., & Liu, X.-H. (1996). Grain size dependence of anatase-to-rutile structural transformation in gel-derived nanocrystalline titania powders. *Journal of Materials Science and Letters*, *15*, 1789.

Dobbins, R. A., & Megaridis, C. M. (1991). Absorption and scattering of light by polydisperse aggregates. *Applied Optics*, *30* (33), 4747.

DuFaux, D. P., & Axelbaum, R. L. (1995). Nanoscale unagglomerated non-oxide particles from a sodium coflow flame. *Combustion and Flame*, *100*, 350–358.

Ehrman, S. H., Friedlander, S. K., & Zachariah, M. R. (1998). Characteristics of SiO2/TiO2 nanocomposite particles formed in a premixed flat flame. *Journal of Aerosol Science*, *29*, 687–706.

Emel'yanov, V. I., Konov, V. I., Tokarev, V. N., & Seminogov, V. N. (1989). Formation of periodic surface ripples under the action of pulsed carbon dioxide laser radiation on fused silica. *Journal of the Optical Society of America B*, *6* (1), 104.

Farias, T. L., Carvalho, M. G., Koylu, U. O., & Faeth, G. M. (1995). Computational evaluation of approximate Rayleigh–Debye–Gans/Fractal-Aggregate theory for the absorption and scattering properties of soot. *ASME Journal of Heat Transfer*, *117*, 152.

Farias, T. L., Koylu, U. O., & Carvalho, M. G. (1996). Range of validity of the Rayleigh–Debye–Gans theory for optics of fractal aggregates. *Applied Optics*, *35* (33), 6560.

Fox, M. A., & Dulay, M. T. (1993). Heterogeneous photocatalysis. *Chemical Reviews*, *93*, 341–357.

Gleiter, H. (1989). Nanocrystalline materials. *Progress in Materials Science*, *33*, 223–315.

Gribb, A. A., & Banfield, J. F. (1997). Particle size effects on transformation kinetics and phase stability in nanocrystalline TiO_2. *American Mineralogist*, *82*, 717–728.

Hwang, J. Y., Gil, Y. S., Kim, J. I., Choi, M., & Chung, S. H. (2001). Measurements of Temperature and OH Radical Distributions in Silica Generating Flames Using CARS and PLIF. *Journal of Aerosol Science*, *32*, 669–681.

Jeong, J. I., & Choi, M. (2001). A sectional method for analysis of growth of polydisperse non-spherical particles undergoing coagulation and coalescence. *Journal of Aerosol Science*, *32*, 633–650.

Jullien, R., & Botet, R. (1987). *Aggregation and fractal aggregates*. Singapore: World Scientific.

Katzer, M., Weber, A. P., & Kasper, G. (2000). On the effects of electrical fields on charge and size distributions of titania particles formed in a flame. Submitted for publication.

Klug, H. P., & Alexander, L. E. (1974). *X-ray diffraction procedures for polystalline and amorphous materials* (2nd ed.). New York: Wiley.

Koylu, U. O., & Faeth, G. M. (1994). Optical properties of overfire soot in buoyant turbulent diffusion flames at long residence times. *ASME Journal of Heat Transfer*, *116*, 152.

Koylu, U. O., Faeth, G. M., Farias, T. L., & Carvalho, M. G. (1995a). Fractal and projected structure properties of soot aggregates. *Combustion and Flame*, *100*, 621–633.

Koylu, U. O., Xing, Y., & Rosner, D. E. (1995b). Fractal morphology analysis of combustion-generated aggregates using angular light scattering and electron microscope images. *Langmuir*, *11*, 4848–4854.

Kruis, F. E., Fissan, H., & Peled, A. (1998). Synthesis of nanoparticles in the gas phase for electronic, optical and magnetic applications-a review. *Journal of Aerosol Science*, *29*, 511–535.

Martin, J. E., & Hurd, A. J. (1987). Scattering from fractals. *Journal of Applied Crystallography*, *20*, 61–78.

Lee, D., & Choi, M. (2000). Control of size and morphology of nanoparticles using CO_2 laser during flame synthesis. *Journal of Aerosol Science*, *31*, 1145–1163.

Lee, B. W., Jeong, J. I., Hwang, J. Y., Choi, M., & Chung, S. H. (2001). Analysis of growth of non-spherical silica particles in a counterflow diffusion flame considering chemical reaction, coagulation and coalescence. *Journal of Aerosol Science*, *32*, 165–185.

Matsoukas, T., & Friedlander, S. K. (1991). Dynamics of aerosol agglomerate formation. *Journal of Colloid Interface Sciences*, *146*, 495.

Mezey, E. J. (1966). In C. F. Powell, J. H. Olxey, & J. M. Blocher (Eds.), *Vapor deposition* (p. 423). New York: Wiley.

Seto, T., Hirota, A., Fujimoto, T., Shimada, M., & Okuyama, K. (1997). Sintering of polydisperse nanometer-sized agglomerates. *Aerosol Science and Technology*, *27*, 422–438.

Shannon, R. D., & Pask, J. A. (1964). Topotaxy in the anatase-rutile transformation. *Americal Mineralogist*, *49*, 1707–1717.

Shannon, R. D., & Pask, J. A. (1965). Kinetics of the anatase-rutile transformation. *Journal of the American Ceramic Society*, *48*, 391.

Siegel, R. W. (1994). *Nanophase materials: synthesis, structure and properties.* F. E. Fugita (Ed.), (p. 65–102). Springer series in Material Sciences.

Sorensen, C. M., Cai, J., & Lu, N. (1992). Light-scattering measurements of monomer size, monomers per aggregate, and fractal demension for soot aggregates in flames. *Applied Optics*, *31*, 6547–6557.

Spurr, R. A., & Myers, H. (1957). Quantitative analysis of anatase-rutile mixtures with an X-ray diffractometer. *Analytical Chemistry*, *29*, 760.

Vemury, S., & Pratsinis, S. E. (1995). Corona-assisted flame synthesis of ultrafine titania particles. *Applied Physics and Letters*, *66*, 3275–3277.

Windeler, R. S., Friedlander, S. K., & Lehtinen, K. E. J. (1997). Production of nanometer sized metal oxide particles by gas phase reaction in a free jet I. *Aerosol Science and Technology*, *27*, 174.

Zhang, H., & Banfield, J. F. (1998). Thermodynamic analysis of phase stability of nanocrystalline titania. *Journal of Materials Chemistry*, *8*, 2073–2076.

Zhang, H., & Banfield, J. F. (1999). New kinetic model for the nanocrystalline anatase-to-rutile transformation revealing rate dependence on number of particles. *American Mineralogist*, *84*, 528–535.